Nanoscale

Accepted Manuscript

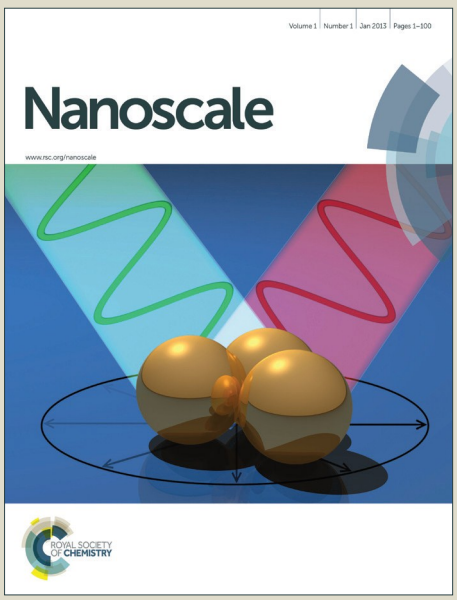

ROYAL SOCIETY OF CHEMISTRY

www.rsc.org/nanoscale

Nanoscale

PAPER

Bioresponsive carbon nano-gated multifunctional mesoporous silica for cancer theranostics

Received 00th January 20xx,
Accepted 00th January 20xx

DOI: 10.1039/x0xx00000x

www.rsc.org/nanoscale

Rajendra Prasad[a, b], Sandhya Aiyer[b], Deepak S. Chauhan[c], Rohit Srivastava[c], Kaliaperumal Selvaraj[a, b]*

Designing bioresponsive nanocarriers for controlled and efficient intracellular drug release for cancer therapy is a major thrust area in nanomedicine. With a recent recognition of US FDA as safe material for human trials, mesoporous silica nanoparticles (MSNPs) are being extensively explored as promising theranostic agents. Green fluorescent carbon quantum dots (CQDs), though known as possible alternates for their more toxic and relatively less efficient predecessors, are less known as gate keepers for drug release control. We report for the first time, an efficient bioresponse of CQDs when judiciously designed using glutathione cleavable (redox responsive) disulphide bonds. When anticancer drug, doxorubicin loaded MSNPs are capped with these CQDs, they display promising drug release control on exposure to mimicked intracellular cancer environment. Their dual functionality is well established with good control on preventing the premature release and exceptional bio-imaging of HeLa cancer cells. Flourescence images prove selective targeting of HeLa cells by over expression of folate receptors from the surface functionalised folic acid ligand. Extensive characterisation using XRD, TEM, BET analysis, drug loading tests, drug release kinetics, MTT assay and fluoroscence cell imaging helps in understanding the multifunctionalities of the successful design, extending its scope with exciting prospects towards non-invasive targeted drug delivery and bio-imaging for effective cancer diagnosis and treatment.

Introduction

Research pertaining to composite nanomaterials have taken on an exciting new dimension in the past decade registering major breakthroughs in fields as diverse as nanomedicine and energy technology.[1-5] Nanomedicine have introduced several novel metal, metal oxide nanoparticles and their inorganic composites for gamut of biomedical functions including controlled, targeted drug delivery and diagnostics.[6-8] However, a major challenge is to design bioresponsive multifunctional theranostic (MFT)/ drug delivery system comprising of various function-specific components to synergistically promote improved site specific chemotherapy and thereby reducing the side effects. In recent years, mesoporous silica (MS) nanoparticles are seen as promising candidates for drug delivery systems due to advantages viz., large surface area, ordered uniform pores, high pore volume and surfaces (both exterior and interior) that are easily functionable with biomolecules and targeting ligands thereby enhancing the biocompatibility too.[9-18] A nanodot of this material has recently been approved by United States Food and Drug Administration (FDA) as safe material for human trials to be tested as first investigational new drug (IND) application for molecular biomedical imaging.[7,8,19-21] A series of mesoporous silica nanoparticles (MSNPs) have been synthesized for various applications including drug delivery, gene delivery apart from other generic applications viz., catalysis, CO_2 capture, etc.[11-16, 22-27] The architectural control and surface functionalization of MSNPs have brought new possibilities for targeted drug delivery and bio-imaging.[18, 26-33] So far, various MSNPs based drug delivery systems with organic (supramolecules)[26, 28, 31] and inorganic gatekeepers (metal nanoparticles)[30] have been developed for the prevention of premature drug release and controlled drug delivery. Stoddart and Zink earlier conceptualized stimuli responsive gatekeepers by using supramolecular nanovalves on MS nanoparticles[23, 26, 28, 34] and in general, nanocarrier systems that respond to either extracellular or intracellular stimuli such as light[23], temperature[23, 28], pH[9, 28, 34] and enzyme.[28, 30] Among these individual stimuli, pH and redox-responsive release mechanisms have been recognized as effective ones for controlled drug release at target sites.[23, 26, 34]

A contemporary thrust area is to explore stable, efficient and safe nanolight agents for biomedical imaging and integrating them in to

[a]Academy of Scientific and Innovative Research (AcSIR), National Chemical Laboratory, Pune-411008, India
[b]Nano and Computational Materials Lab, Catalysis Division, CSIR-National Chemical Laboratory, Pune-411008, India
[c]Department of Bioscience and Bioengineering, IIT Bombay, Powai, Mumbai, 400076, India
Email: k.selvaraj@ncl.res.in, kselva@gmail.com

Electronic Supplementary Information (ESI) available: Size distribution histograms, PL spectra of CQDs at different pH and different excitation wavelength, TEM images and FTIR spectrum See DOI: 10.1309/x0xx0000x

such multifunctional systems.[29, 35-38] Many fluorescent organic dyes and quantum dots (QDs) have been independently attempted for bioimaging.[38-40] However, due to several strong demerits, they are far from *in vivo* applications.[39, 40] To mention a few, semiconductor and metal QDs owing to poor photostability, photo-blinking and poor biocompatibility.[41, 42] Recently, carbon and graphene quantum dots, a new class of fluorescent materials, have attracted many researchers for their exploitation in bio-sensing and bio-imaging.[35-36] As compared to other quantum dots and organic dyes, carbon quantum dots (CQDs) are superior in properties such as good luminescence, photostability, water solubility and biocompatibility making them suitable for biomedical applications.[37-42] Many methods have been proposed to prepare CQDs which are classified into "Top-down" and "Bottom-up" approaches and their modification can be achieved by synthesis processes.[43-53] For example, Ajayan and coworkers have reported different fluorescent graphene QDs with blue, green and yellow fluorescence.[54] Despite many achievements, understanding their other possible functions and the feasibility to be included in a multifunctional system are yet to be realised. They remain as major challenges in biomedical research due to complexities in synthetic fabricating steps and yet maintaining their performances.

Upsurge concerns over issues such as toxicity and bio-compatibility are often obvious in case of using several functional components. However, integrating them in to a single system, strongly suppresses them. For instance, apart from its role in bioimaging, a fluorescent material may also perform a role of gate keeping. The present article successfully reports such a design where mesoporous silica nanoparticles (MSNPs), used as nanocarriers for anticancer drug, are capped with CQDs that play dual roles viz., (i) nanolight agent for site-specific bioimaging and (ii) efficient gatekeepers to prevent the premature drug release facilitating targeted delivery. In specific, the present work demonstrates a remarkable bioresponsive gatekeeping ability of CQDs for the first time. In recent literature, very few reports on MSNPs capped with CQDs are available. Qu and coworkers have attempted to cap MSNPs with CQDs, however, with a significant premature release of anticancer drug, doxorubicin (DOX).[33] This issue has been later addressed to a larger extent by Fu and coworkers using graphene quantum dots (GQDs) to cap MSNPs.[34] These scanty reports published in this respect rather suggest the huge scope of further explorations in terms of issues viz., improving the pore sealing to further reduce premature drug release, reducing the number of synthesis steps involved, etc. The disparity between pore diameter and size of quantum dots used for capping may result in loosely sealed pores which may be attributed to the premature drug release. In addition, while these articles mainly report pH based response, the significance of elevated glutathione (GSH) concentration, an evident characteristic factor of cancer cells from normal ones has never been exploited in gate keeping by using CQDs. This paper reports a successful design of bioresponsive CQDs capped MSNPs based targeted nanocarrier for bioimaging of cancer (HeLa) cells and its controlled intracellular delivery of DOX when subjected to a mimicked cancer cell environment.

Results and discussion

An objective of this work is to check the feasibility of fabricating such a systems using inexpensive CQDs synthesized through simple synthesis route from natural sources and yet achieving the performances compared to that of the relatively expensive GQDs. Fluorescent quantum dots are obtained from graphene oxide (GQDs) from Graphite (procured from Sigma Aldrich) and natural source, sugarcane waste (CQDs). The synthesized GQDs and CQDs have particle size ~ 6 nm and ~ 5 nm respectively along with thickness of ~ 1.5 nm and 1 nm, respectively (from the AFM images obtained in tapping mode, Fig. 1). The green fluorescent nature of both QDs is confirmed by photoluminescence (PL) spectra showing emission ~ 530 nm with 470 nm excitation wavelength. Digital photographs of QDs indicate their green fluorescent nature and their better dispersion ability in aqueous media (Fig. 2). The extensive characterization carried out on both QDs proves that there is almost no difference between them in terms of their optical properties. Hence, the green fluorescent CQDs are employed as bioresponsive gatekeepers in the present work to assess their ability to prevent the premature release of DOX and also to be as efficient marker for bio-imaging of human cancer cells. Notably, these CQDs are synthesized at ambient conditions unlike reported in the literature and this synthesis route from natural sources is reported here for the first time.

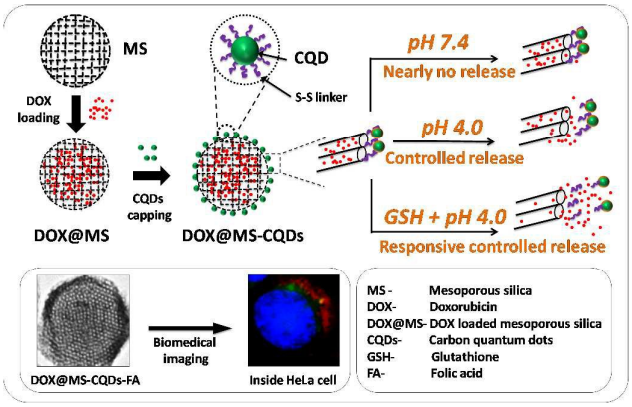

Scheme. 1 Schematic showing bioresponsive dual functional CQDs capped MS.

A brief description of the functional design of the proposed system is discussed here (scheme 1). Green fluorescent CQDs are capped onto the openings of the DOX loaded pores of MSNPs by using GSH sensitive disulphide bonds[28] (MS-CQDs). MS-CQDs nanoparticles on exposure to a cancer mimicked intracellular environment, release of drug is expected as the cystamine disulphide bonds are cleaved in response to the excess glutathione concentrations (2-20 mM).[55-57] Intracellular glutathione concentrations of normal cells are generally lesser by an order compared to that of cancer cells.[58-61] At extracellular conditions in physiological pH (7.4), the amine functionalized green fluorescent CQDs are tightly attached onto the MSNPs by electrostatic interactions thus sealing the pores and preventing the premature release of DOX. However, in acidic pH the protonation causes electrostatic disturbance and thus loosening of the CQDs caps from the MSNP pore openings leading to release of

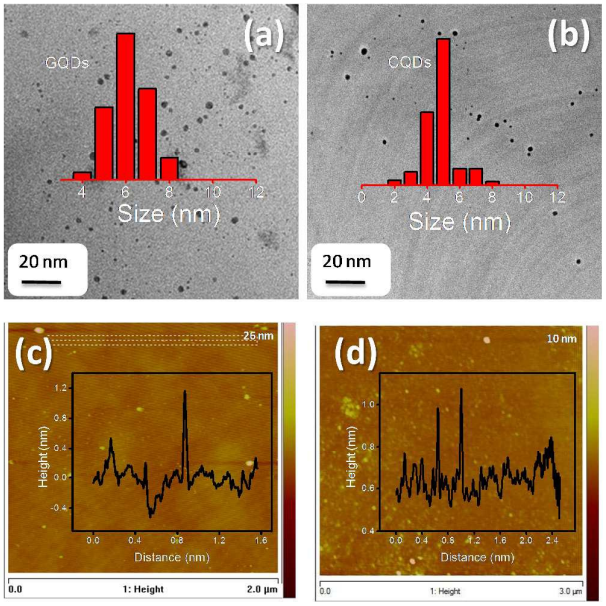

Fig. 1 TEM images of (a) graphene quantum dots (GQDs), (b) carbon quantum dots with their particle size histograms, AFM images of (c) GQDs and (d) CQDs with their height profiles

DOX. In general, the amount of drug release depends upon the nature of release medium.[56, 59, 62] A successful bioresponse is indicated by further release of DOX on exposure to a release medium of pH 4 along with elevated concentrations of GSH. This is due to rapid cleavage of disulphide bonds and weakening of electrostatic interactions on MSNPs surface due to protonation in acidic pH respectively.

MS nanoparticles are synthesized according to a reported method with some modifications[9, 10] and pores are capped by green fluorescent CQDs. 1-ethyl-3-(3-dimethylaminopropyl) carbodiimide (EDC) and N-hydroxysuccinimide (NHS) are used to activate the carboxylic groups present on green fluorescent CQDs. The treatment of these activated CQDs with disulphide bond containing cystamine (Cyst) resulted into cystamine functionalized CQDs (CQDs-Cyst) which is further attached onto the surface of mesoporous silica via electrostatic interactions giving green fluorescence CQDs capped MSNPs. Highly dispersed spherical MSNPs covered by CQDs with sizes of ~ 100 nm and ~ 5 nm respectively are observed from the TEM images (Fig. 3 a-f) and particle size distribution histogram profiles (ESI Fig. S1). It is also evident (from the AFM image of CQDs obtained in tapping mode) that the thickness of the majority of dots is approximately 1 nm which corresponds to a single-layered dispersion of CQDs (Fig. 1). The presence of ordered hexagonal arrays of mesopores in MSNPs and MS-CQDs are further confirmed by TEM images and XRD patterns. The MSNPs show clear lattice fringes which are diminished to an extent upon capping with CQDs (Fig. 3 a, c) and reappear in the images of MSNPs taken after the detachment of CQDs (Fig. 3 e, f).

The gap calculated between lattice fringes of MSNPs also confirms this (ESI Fig. S2 a, b). Low angle powder X-ray diffraction (LAPXRD) pattern is used to determine the mesophase structures of MSNPs,

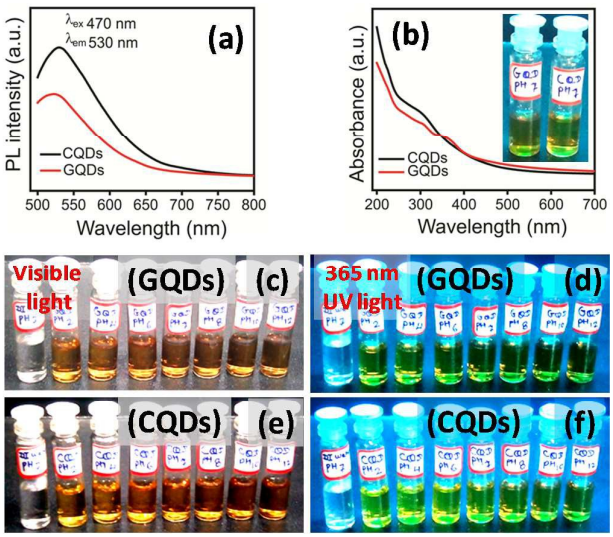

Fig. 2 (a) PL spectra, (b) absorption spectra of GQDs and CQDs, digital photographs (c-f) of GQDs and CQDs at different pH in aqueous media

MS-CQDs and MS-CQDs-FA nanoparticles (Fig. 4 a). Four characteristic reflections for the diffraction planes (*100, 110, 200, 210*) of mesoporous silica (MCM-41) are observed at respective diffraction angles (2θ) 2.3°, 4.0°, 4.5° and 6.2° indicating the existence of highly ordered 2D hexagonal array of mesopores.[9, 10] Slight shift in diffraction planes and reduction of respective peak intensities are observed in case of MS-CQDs which are attributed to functionalization and subsequent pore capping. The disappearance of diffraction planes (*110, 200, 210*) on further attachment of folic acid (FA) to MS-CQDs nanoparticles is consistent with the literature.[9, 32] These particles are well dispersed and stable. This is confirmed by testing the dispersity of these particles in various media such as simulated body fluid (SBF), phosphate buffered saline (PBS) and saline for a period of 24 h and by using dynamic light scattering (DLS) measurement. More details are available in ESI Fig. S3 (digital

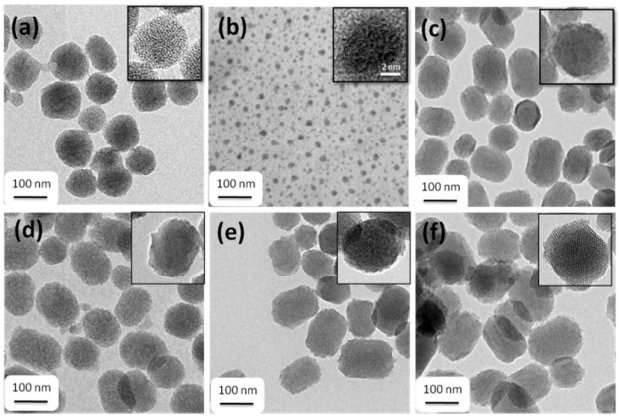

Fig. 3 TEM images of (a) mesoporous silica (MS), (b) CQDs, (c) CQDs capped MS, (d) folic acid attached CQDs capped MS, (e) before CQDs detached MS and (f) after CQDs detached MS, inset single particle of each.

photographs) and Fig S4. (average particle size histogram from DLS) with acceptable range of polydispersity index (PDI) as shown in Table S1. From combined TEM and XRD analysis it is concluded that surface functionalization of MS and its pore capping with CQDs have no destructive impact on the mesoporous structure. The above observations in XRD are summarized in tabular form (ESI Table S2).

Nitrogen adsorption-desorption isotherms of MS nanoparticles, MS-CQDs and MS after CQDs detached are shown in Fig.4 b. It is evident that MSNPs follows a typical IV isotherm having surface area 1058 m^2/g with ~ 3 nm pore diameter. A drastic reduction in BET surface area (from 1058 to 154 m^2/g) a change in the shape of the isotherm from type IV to type I (after CQDs capping) and a drop in pore volume (from 0.9 to 0.2 cm^3/g) are observed when MS pores are capped with CQDs thus confirming their tight sealing. Detachment of CQDs from sealed pores under acidic pH along with elevated concentrations of GSH (10 mM), is evident from the significant increase in the surface area (from 154 to 785 m^2/g) and in pore volume (from 0.2 to 0.5 cm^3/g). This further confirms the pore sealing is effective. This highly effective pore sealing is attributed to the ideal size match between that of the MS pores (~ 3 nm) and CQDs (~ 5 nm) unlike trials attempted earlier in literature. The summary of BET measurements is provided in supporting information (ESI Table S3).

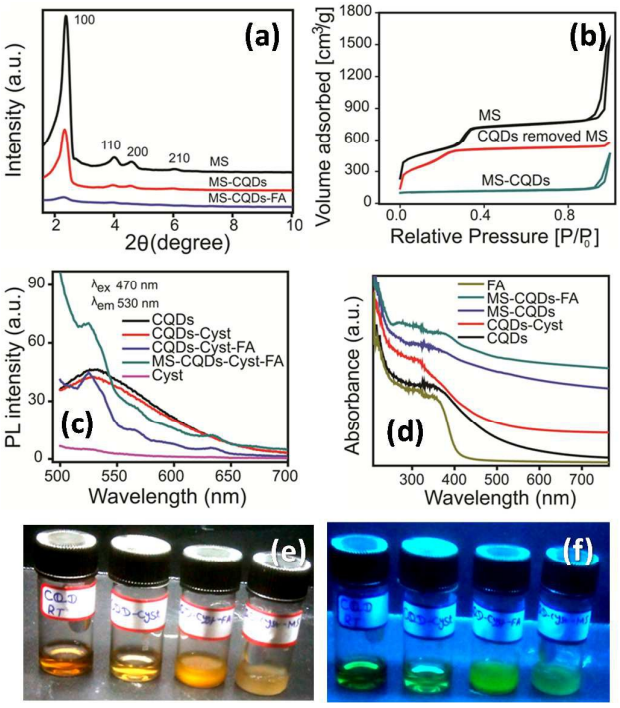

Fig. 4 (a) PXRD patterns of MS, MS-CQDs and MS-CQDs-FA, (b) BET isotherms of MS, MS-CQDs and CQDs detached MS, (c) PL spectra of CQDs, Cystamine functionalized CQDs (CQDs-Cyst), folic acid functionalized CQDs-Cyst (CQDs-Cyst-FA), CQDs-Cyst-FA capped MS and Cystamine (Cyst) and (d) absorption spectra of CQDs and CQDs capped MS with digital photographs (e and f) of CQDs, CQDs-Cyst, CQDs-Cyst-FA and MS-CQDs-Cyst-FA

The efficacy of pore sealing is checked once again with doxorubicin (DOX) loading tests carried out on MS and MS-CQDs (the quantum of DOX loaded or released are calculated using the linear equilibrium curve of drug and the equations (ESI eq.S1 and eq.S2) for drug loading amount and efficiency; see Fig. S5 in ESI). MS shows 28 % loading efficiency before pore sealing and the loading efficiency is as lowest as ~ 5 % (apparently due to the external surface) for MS-CQDs where the pores are sealed with

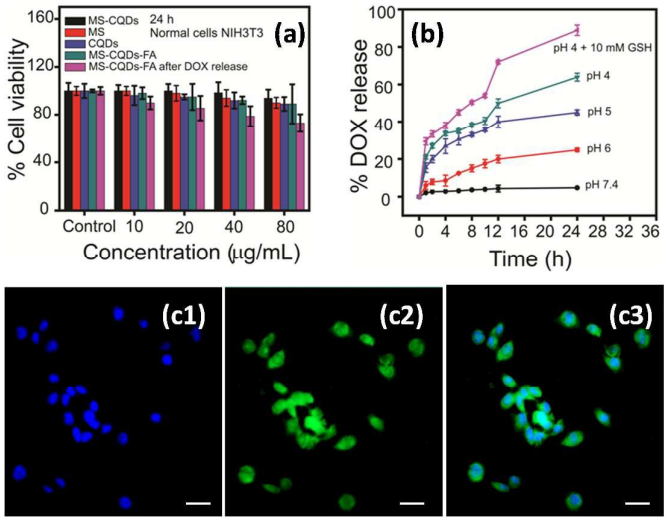

Fig. 5 (a) % Cell viability by MTT assay of CQDs, MS, MS-CQDs, MS-CQDs-FA and MS-CQDs-FA after DOX release with NIH-3T3 normal cell, (b) time dependent drug release profiles at different release media and targeting ability of MS-CQDs-FA on HeLa cells through fluorescence microscopy images, (c1) DAPI stained nucleus in blue, (c2) presence of CQDs inside the cell emitting green fluorescence and (c3) merged fluorescence, scale bar is 40 μm.

CQDs (from UV-Vis absorbance spectroscopy data; see Fig. S6 in ESI) corroborating the BET data. To check if the process of sealing with CQDs results in any loss of DOX, the samples before and after the process are tested with UV-Vis and also PL and the loss is calculated to be a meagre ~3 % (details are available in ESI; Fig S7, Table S4 and ESI eq.S1 and eq.S2). UV source in cabinet is used for preliminary screening of fluorescence behavior of CQDs, MS-CQDs and MS-CQDs-FA (Fig. 4 c, e and f). The green fluorescent nature of CQDs, CQDs-Cyst, CQDs-Cyst-FA and MS-CQDs-FA is confirmed by photoluminescence (PL) spectra showing emissions at 530 nm with 470 nm excitation wavelength (Fig. 4 c), thus making them promising substrate for *in vitro* and *in vivo* bio-imaging (PL at different pH and excitation wavelength in ESI Fig. S8). In the absorption spectra of CQDs, CQDs-Cyst, CQDs-Cyst-FA and MS-CQDs-FA (Fig. 4 d), the peaks centered at λ_{max} 220 nm and 340 nm correspond to π-π^* transition of the C=C band and n-π^* transition of C=O band respectively. In addition to the above peaks, folic acid functionalized MS-CQDs show absorption peaks at 290 and 360 nm which are significant peaks of FA thus, confirming the successful attachment of FA with green fluorescent CQDs.

Additionally, the O−H stretching vibrations (3426 cm^{-1}) and the C=O stretching vibrations (1697 cm^{-1}) in FT-IR spectra confirm carboxyl groups on CQDs. Peak at 1620 cm^{-1} corresponding to -NH_2 bending vibrations of the cystamine moiety reveals successful functionalization of cystamine on CQDs. Peaks at 2824 and 2933 cm^{-1} corresponding to –C-H stretching vibrations. The IR bands between 800-1180 cm^{-1} correspond to Si-O-Si stretching[62] whereas the bands between 1413-1507 cm^{-1} indicate stretching vibrations of the aromatic rings of folic acid moieties (see Fig. S9 in ESI).

MTT assay with NIH-3T3 normal cell-line is used for *in vitro* cytotoxicity studies of CQDs, MS, MS-CQDs, MS-CQDs-FA and MS-CQDs-FA after DOX release prior to their bio-medical applications. More than 90 % cell viability is observed even at concentrations upto 80 µg/mL of CQDs, MS, MS-CQDs, folic acid functionalized MS-CQDs (MS-CQDs-FA). A cell viability of 73% has been observed for the sample MS-CQD-FA after DOX release and the insignificant reduction of viability is attributed to the further loss of biocompatibility due to the removal of surface functionalized species such as CQDs, FA etc., during the release of DOX (Fig. 5 a). To prove the redox-responsive gatekeeper behavior of CQDs on the MS surface, anticancer drug DOX is chosen for loading and release kinetics (see Fig. S10 and eq. S1-3 in ESI).

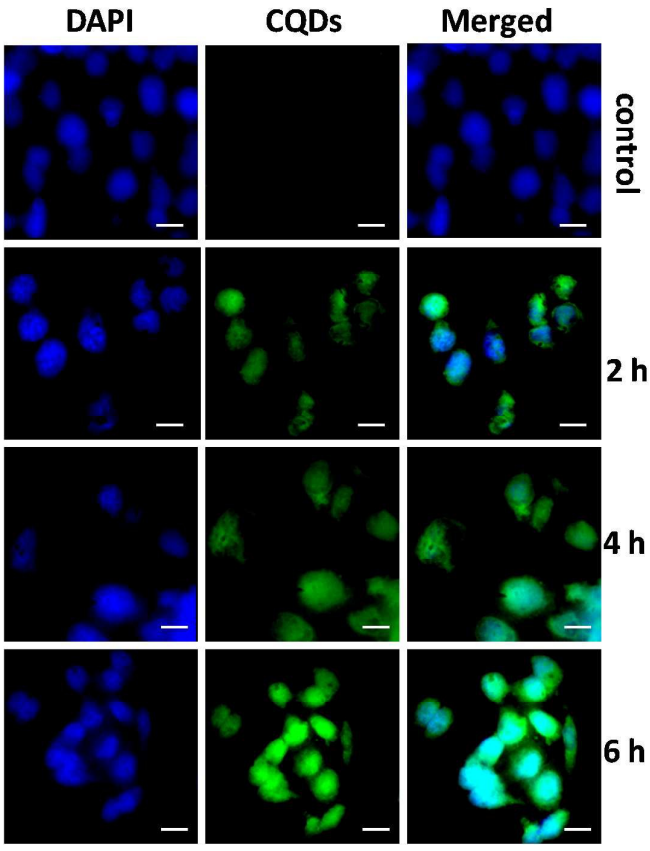

Fig. 6 Distribution and visibility of detached green fluorescent CQDs from MS-CQDs-FA in HeLa cells through dual responsive cleavage (pH and GSH), fluorescence microscopy images with different incubation time, DAPI stained nucleus in blue, detached CQDs in cell interior with green fluorescence and merged fluorescence. All images are with 20 µm scale bar.

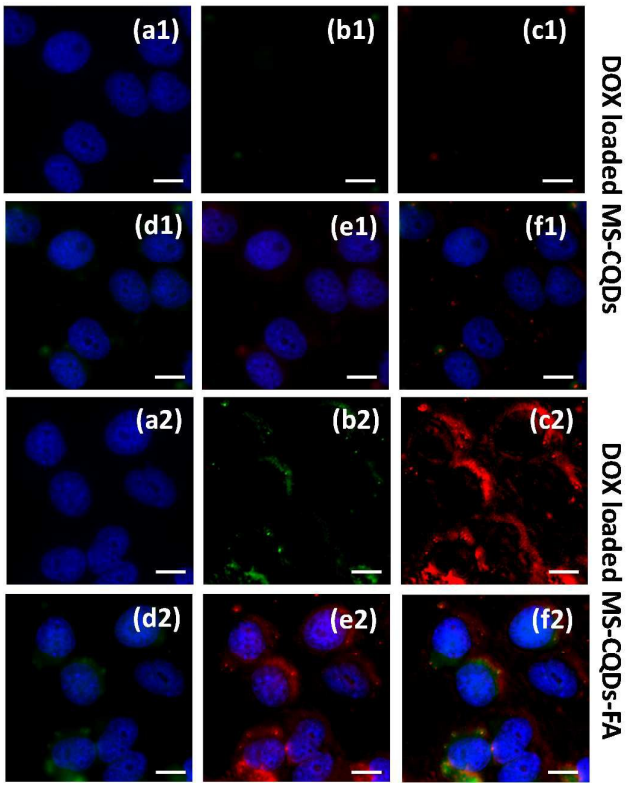

Fig. 7 Cell uptake and distribution of DOX in HeLa cells when cells are incubated with 40 µg/ mL of DOX loaded MS-CQDs (a1-f1) and MS-CQDs-FA (a2-f2) for 2 h. Due to targeting, Intra cellular localization of DOX loaded MS-CQDs-FA was fast compared to DOX @MS-CQDs. Fluorescence microscopy imaging of treated cells, DAPI stained nucleus (blue a1,a2), CQDs (green b1, b2), DOX (red c1,c2), merged fluorescence of blue and green (d1, d2), merged fluorescence of blue and red (e1, e2) and merged fluorescence of blue, green and red (f1, f2). All images are with 10 µm scale bar.

Though literature reports the use of pH 7.4 and 4 to mimic the extracellular and deep intra cellular late endosomal environments respectively in general[63-65] release kinetics are tested for a period of 24 h at various pH as 7.4, 6, 5 and 4 to get a deeper insight about the drug release capabilities at various stages of intracellular uptake. In addition to that, pH 4 along with 10 mM GSH to mimic deep intracellular and late endosomal conditions especially where the excess concentration of GSH can trigger the disulphide bond cleavage based drug release is also tested. Release kinetics data at all the mentioned conditions are shown in Fig. 5b. An insignificant 4.3 % of release at neutral pH even after 24 h shows the best possible sealing of the pores and that the design is successful with the effective control on premature drug release at extracellular and normal physiological conditions. However, as the MFT agent enters into the cell where the pH range falls to ~ 6 the release goes up steadily to 24.8 % and doubles with a difference of ~ 20 % to about 45 % as the pH further falls to 5. For a deep intracellular environment where the pH dips down to 4, the release is about 63.9 % with a difference of about 20 % again. A late endosomal condition as mimicked by a reduced pH of 4 along with 10 mM GSH almost doubles (88.9 %) the difference in the raise of the release of

DOX at pH 4 without GSH. It is also interesting to note that the GSH based bioresponsive release is prominently observed after 12 h. Though, the disulphide bond cleavage based mechanism is reported in literature with other systems, [55, 57-59], this clear demonstration of the bio-responsiveness of a judicious design with green CQDs is in this way, to the best of our knowledge, is a first ever report. To evaluate the bio-imaging and targeting ability of fluorescent payload nanomaterials, HeLa cells are cultured in physiological conditions and incubated with 40 µg/ mL of MS-CQDs-FA, DOX loaded MS-CQDs and DOX loaded MS-CQDs-FA. The green fluorescence by MS-CQDs-FA after 2 h incubation with HeLa cells considerably gives primary indication of targeting ability (Fig.5c1-3). Further, the visibility of green fluorescence increase with incubation time (2, 4 and 6 h) of MS-CQDs-FA with HeLa cells when compared to control (without MS-CQDs-FA nanoparticles) (Fig. 6) confirming their efficient bio-imaging ability and thus strengthens their candidature as cell markers. Moreover, the enhanced visibility of green fluorescence after 6 h attributes superior intracellular delivery. Further to understand the effectiveness of targeting and successive intracellular delivery of DOX, the fluorescence microscopy images of incubated (2 h) HeLa cells are collected for blue (DAPI), green (CQDs) and red (DOX) (Fig. 7). Images shown in Fig. 7 a1-f1, show the poor intracellular uptake of DOX by HeLa cells as the targeting ligand (FA) is absent, while that of DOX is significantly observed through the bright red color as shown in Fig. 7 a2-f2, which explain the enhanced intracellular uptake due to the presence of functional FA ligand. The increase in green and red florescence in the second set of images (a2-f2) clearly indicates the effective targeting due to functional ligand, FA and successive intracellular delivery of DOX. In addition, to understand the extent of intracellular uptake at extended incubation periods, additional experiments are carried out for a period of up to 18 h with DOX@MS-CQD-FA on HeLa cancer cell lines. Fluorescence images clearly show that as the incubation time increases, the intracellular delivery of DOX and its availability in the cell nuclei are constantly increasing (Fig 8, Refer Fig. S11 in ESI for better comparison).

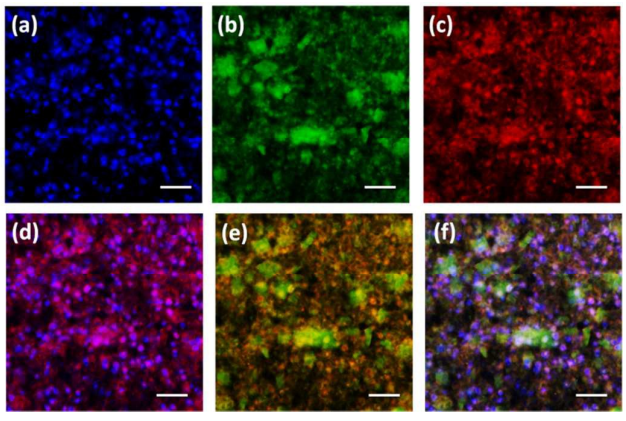

Fig. 8 Cell uptake and distribution of DOX in HeLa cells when cells are incubated with 40 µg/ mL of DOX@MS-CQDs-FA for 18 h. Fluorescence microscopy imaging of treated cells, DAPI stained nucleus (blue, a), CQDs (green, b), DOX (red, c), merged fluorescence of blue and red (d), merged fluorescence of green and red (e) and merged fluorescence of blue, green and red (f). Images are with 100 µm scale bar.

The drug release curve and fluorescence imaging experiments significantly indicate no leakage of drug (DOX) which is desirable in order to reduce side effects of anticancer drugs on normal cells. Therefore, present nano-carrier clearly demonstrates the prevention of premature leakage. Further, the fluorescence studies showing the presence of drug inside the cells can be attributed to the successful intracellular release of drug by nano-carrier. The targeted release further suggests that disulphide bonds are bio-responsive as observed in release kinetics data (Fig. 5 b) and that their cleavage leads to pore opening followed by the release of DOX inside the cancer cells. As a follow up of this work, a detailed in-vivo study with the bioresponsive nanocarrier system to understand the true intracellular release and anticancer activity is currently being planned and the results will be published in future.

Experimental section

Materials and characterization techniques

N-cetyltrimethylammonium bromides (CTAB), tetraethylorthosilicate (TEOS), dimethylsulphoxide (DMSO), sodium hydroxide (NaOH), sulphuric acid (98.08 % H_2SO_4) and nitric acid (70 % HNO_3) are purchased from Merck limited, Mumbai, India. Graphite powder, 1-ethyl-3-(3-dimethylaminopropyl) carbodiimide (EDC), N-hydroxysuccinimide (NHS), folic acid (FA), citric acid, cystamine dihydrochloride, glutathione and 3-(4, 5-dimethylthiazol-2-yl)-2, 5-diphenyltetrazolium bromide (MTT) are purchased from Sigma–Aldrich Pvt. Ltd., USA. Sodium carbonate (Na_2CO_3, 99.9 %) is purchased from Fischer Scientific limited Mumbai, India. Dulbecco's modified Eagle's medium (DMEM), fetal bovine serum (FBS), phosphate-buffered saline (PBS), antibiotic-antimycotic solution are procured from HiMedia Laboratories Pvt. Ltd., India. Quantum dots are obtained from graphene oxide and sugarcane carbon powder. Milli-Q grade water ((Millipore) > 18.2 MΩ cm) is used for all experiments. Synthesized carbon quantum dots (CQDs) are systematically characterized with various physicochemical techniques. The size and morphology of nanostructures are examined by transmission electron microscopy (TEM FEI Tecnai T-20) operating at 200 kV. Samples for TEM are prepared by evaporating a droplet of sample onto 200 mesh carbon coated copper grid. Optical properties of CQDs, MS-CQDs NPs (Carbon quantum dots capped mesoporous silica nanoparticles), MS-CQDs-FA NPs (Folic acid conjugated carbon quantum dots capped mesoporous silica nanoparticles) are characterized by UV/visible/NIR (Jasco V570) and photoluminescence (Scinco, Korea) spectrophotometer using standard quartz cuvette having a path length of 1 cm . A Zetasizer ZS 90 apparatus utilizing 633 nm red laser (at 90° angle) from Malvern instruments is used for DLS measurements. A minimum of three readings are collected using freshly prepared samples in PBS, saline and SBF solutions. Powder XRD (PXRD) patterns of nanostructures are recorded using a PANalytical X'pert pro dual goniometer diffractometer. The data are collected with a step size of 0.008° and scan rate of 0.5° min^{-1} by using Cu Kα (λ = 1.54 Å) radiation source. Fourier transform infrared (FT-IR) spectra are recorded by using Perkin-Elmer FT-IR spectrum GX instrument. KBr crystals are used as the matrix for preparing

samples. The N_2 adsorption-desorption isotherms are recorded using Quantachrome Quadra Win Instrument. The specific surface area is calculated using the Multiple point Brunauer–Emmett–Teller (BET) theory. Pore volume is estimated at a relative pressure of P/P_o = 0.99. Barrett–Joyner–Halenda (BJH) analyses are used to calculate the surface area, pore size and pore volume. Digital photographs are captured in UV cabinet. AFM images are obtained from atomic force microscope (PSIA XE- 100) on tapping mode. The samples for AFM measurements are prepared by drop casting on clean silicon wafers surface after ultrasonic treatment (Equitron ultrasonic cleaner). Bio-imaging and intracellular localization of drug and carrier is performed with the help of fluorescence microscope. The fluorescence microscopic images are taken by Carl Zeiss inverted fluorescence microscope model AXIO OBSERVER.ZI using DAPI (350−430 nm blue), Alexa (488−520 green), and rhodamine (480−580 nm red) filters.

Methods

Synthesis of mesoporous silica (MS) nanoparticles

Mesoporous silica nanoparticles (MSNPs) are synthesized according to previously reported procedure with some modifications.[9, 10] In brief; 1 g of N-cetyltrimethylammonium bromide (CTAB) is dissolved in 480 mL of water 3.5 mL of 2 M NaOH aqueous solution is added to the CTAB solution followed by adjusting the solution temperature to 80 °C. 5 mL of Tetraehtylorthosilicate (TEOS) is added drop wise to the surfactant solution under vigorous stirring. The mixture is stirred for 2 h to give a white precipitate. The product is collected via centrifugation (10,000 rpm for 20 min.). Thereafter, it is thoroughly washed with water and methanol. Further, placed under high vacuum at 70 °C for 24 h to remove the remaining solvent from the pores of MSNPs. To remove the surfactant template CTAB, 1 g of the synthesized MSNPs is refluxed with 1 mL of 11.2 M HCL in 100 mL of methanol at 65 °C for 12 h. The resulting material is filtered and thoroughly washed with water and methanol then placed under high vacuum for 24 h at 70 °C temperature.

Synthesis of green fluorescent graphene quantum dots (GQDs)

In a round bottom flask, 100 mg of graphene oxide powder[39] is mixed with 15 mL of concentrated H_2SO_4 and the mixture is left to bath sonicate for 2 h at room temperature. Thereafter, mixture is added into a concentrated solution of H_2SO_4 and HNO_3 prepared at volume ratio of 15:10 and stirred for 24 h at 100 °C. After completion of reaction (24 h), 200 mL water is added and its pH is adjusted to 7 with the help of Na_2CO_3 and NaOH. Reaction solution is left to slowly stir in ice bath for 3 h to remove the salts in the form of precipitation. After that, product is dialyzed using dialysis bag (molecular weight cut-off 2000 Da) for 2 days.

Synthesis and functionalization of green fluorescent CQDs

In a round bottom flask, 100 mg of carbon powder from natural source (carbon powder formed by burning in tube furnace) is mixed with 15 mL of concentrated H_2SO_4 and the mixture is left to bath sonicate for 2 h at room temperature. Thereafter, mixture is added into a concentrated solution of H_2SO_4 and HNO_3 prepared at volume ratio of 15:10 and stirred for 24 h at room temperature. After completion of reaction (24 h), 200 mL water is added and its pH is adjusted to 7 with the help of Na_2CO_3 and NaOH. Reaction solution is left to slowly stir in ice bath for 3 h to remove the salts in the form of precipitation. To introduce carboxyl groups on the surface of CQDs, 10 mg/mL of citric acid and 10 mL of CQDs solution are mixed under stirring and subsequently left for 6 h at room temperature. After that, product is dialyzed using dialysis bag (molecular weight cut-off 2000 Da) for 2 days. The resulting solution is checked for fluorescence by passing UV light in UV cabinet. To functionalize the surface of CQDs with amine group, cystamine dihydrochloride is used. Carboxyl group of CQDs is activated by 1-ethyl-3-(3-dimethylaminopropyl) carbodiimide (EDC) and N-hydroxysuccinimide (NHS) for 24 h. Thereafter, 5 mL of activated CQDs is mixed with 10 mg of cystamine dihydrochloride dispersed in 10 mL of water. Mixture of CQDs and cystamine dihydrochloride is left to vigorous stirring for 12 h at room temperature and subsequent product cystamine conjugated CQDs (CQDs-Cyst) is purified by dialysis.

Synthesis of folic acid conjugated CQDs-Cyst (CQDs-Cyst-FA)

The surface functionalization of CQDs-Cyst with folic acid is carried out stepwise. To activate carboxyl group, 60 mg of 1-ethyl-3-(3-dimethylaminopropyl) carbodiimide and 50 mg of N-hydroxysuccinimide are added in 200 mg of folic acid dissolved in 20 mL of water. After 12 h, 15 mL solution of CQDs-NH_2 (CQDs-Cyst) having conc. of 2 mg/mL is added to the activated folic acid solution and allowed to react at room temperature for 24 h. The activation of folic acid and anchoring on amine functionalized CQDs reactions should be protected from light.

Silica surface decoration with green CQDs and CQDs-FA (MS-CQDs-FA)

Synthesized MSNPs are dried in oven at 120 °C for 12 h. 0.50 g of dried MSNPs are mixed with 5 mL aqueous solution of cystamine functionalized CQDs and left to stir for 24 h at room temperature. CQDs capped mesoporous silica nanoparticles (MS-CQDs NPs) is pelleted down at 5000 rpm for 10 min. Thereafter, thoroughly washed with water and dried under high vacuum at 60 °C for 24 h. The same method is used to synthesize folic acid functionalized CQDs capped mesoporous silica nanoparticles (MS-CQDs-FA).

Drug loading and release studies

Loading efficiency of MSNPs and MS-CQDs-FA NPs are tested with the help of anticancer drug doxorubicin (DOX). DOX is dissolved at conc. of 1 mg/mL in PBS buffer (pH 7.4). 15 mg of surfactant free MSNPs and MS-CQDs-FA NPs are dispersed separately in 5 mL of drug solution. The MSNPs and MS-CQDs-FA nanoparticles are left to stir at room temperature for 24 h. Thereafter, dispersion is centrifuged to collect the drug loaded MSNPs and MS-CQDs-FA NPs. In order to remove drug on the exterior surface of MSNPs and MS-CQDs-FA NPs, they are thoroughly washed with water. The amount of drug loaded into MSNPs and MS-CQDs-FA NPs are calculated by subtracting the amount of drug in the supernatant from the total

amount of drug used. For drug release study, 1.0 mL of DOX loaded MS-CQDs-FA NPs are transferred into a dialysis bag (molecular weight cut-off 12 KD). The bag is subsequently placed in 100 mL of various pH buffer (7.4, 6, 5, 4 and 4 with 10 mM GSH) solutions and left to stir at 37 ℃. At different time intervals, 1 mL solution is collected and replaced with 1 mL of fresh PBS solution to keep volume constant. The amount of DOX in the release medium is measured by UV-Vis spectroscopy at the wavelength of 480 nm.

Detachment of CQDs from silica surface

To detach CQDs from pores of MS-CQDs-FA NPs. 200 mg of MS-CQDs-FA NPs are added in 100 mL of 10 mM glutathione (GSH) solution of pH 4 and kept for vigorous stirring. After 2 h, product is collected by centrifuging at 10,000 rpm for 20 min. Thereafter, it is thoroughly washed with water, methanol and dried under high vacuum at 70 °C for 12 h to yield the CQDs detached MSNPs.

Cell culture

The normal NIH-3T3 cells and HeLa cancer cells are cultured in Dulbecco's Modified Eagle's Medium (DMEM Gibco, Carlsbad, CA, USA) supplemented with 10% Fetal Bovine serum and penicillin/ streptomycin, under 5% CO_2 atmosphere at 37 °C.

In vitro cytotoxicity assay

In vitro cytotoxicity studies are performed over NIH-3T3 cells using 24 h MTT assay. Cells are seeded at density of ~ 10^4 cells per well of 96-well plate. After overnight incubation at 5 % CO_2 and 37 °C, 100 µl of different concentration (10-80 µg/mL) of MSNPs, CQDs, MS-CQDs, MS-CQDs-FA and MS-CQDs-FA after DOX release nanoparticles dispersed in media are added into wells. Following 24 h incubation wells are washed off with PBS and 20 µl of MTT dye is added. Formazan crystals formed after 4 h are dissolved by 200 µL of DMSO. Optical absorbance is recorded at 570 nm and 690 nm using microplate reader (Tecan Infinite 200 PRO). Percentage cell viability is calculated in reference to untreated cells (negative control).

Cellular uptake and tracking of green fluorescent CQDs

To check the cell targeting performance, we have chosen folic acid (FA) as a targeting ligand and HeLa cells are treated with folic acid functionalized MS-CQD. Before this study the HeLa cells seeded in 96 well plate at density of ~10^4 cells/well and incubated overnight in incubator maintained at 5 % CO_2 and 37 °C. Next day, wells are washed off with PBS and 100 µl of 40 µg/mL of MS-CQDs-FA NPs are added. After 2 h, wells are washed off with PBS twice to remove unbound particles. Thereafter, 4 % paraformaldehyde solution is added to the cells and after 10 min of incubation nuclei are stained with 4, 6-diamidino-2-phenylindole (DAPI). Cover slip is then mounted over a drop of 70 % glycerol on glass slide to fix the phase of the cell. Images are captured using fluorescence microscope (Axio Observer Z1, Carl Zeiss). To evaluate the green fluorescence performance of CQDs, HeLa cells are treated with 40 µg/mL concentration folic acid functionalized MS-CQDs for different incubation time (2, 4 and 6 h).

Intracellular localization of DOX using fluorescence microscope

To check localization and distribution of DOX inside cancer cell, HeLa cells are treated with DOX@MS-CQDs and DOX@MS-CQDs-FA for incubation time 2 h and 18 h. Before this study the HeLa cells are grown in Dulbecco's Modified Eagle's Medium (DMEM Gibco, Carlsbad, CA, USA) at the density of 2×10^4 cells/well in 96 well plates and incubated for 24 h. After being rinsed with PBS, the cells are incubated with 40 µg/mL concentration of DOX@MS-CQDs and DOX@MS-CQDs-FA 2 h and 18 h. After incubation for a required interval of time, HeLa cells are washed with PBS twice to get rid of all the unbound particles. Then for each, 4% paraformaldehyde solution is added to the cells and incubated for 10 min and nuclei are stained with 4, 6-diamidino-2-phenylindole (DAPI). The cover slip is then mounted on a drop of 70 % glycerol on glass slide to fix the phase of the cell. The fluorescence images are taken using fluorescence microscope (Axio observer. Z1).

Conclusions

In summary, we have designed a novel bioresponsive dual functional green fluorescent CQDs functionalized mesoporous silica nanoparticles based nano-theronastic agent. The design ensures (1) targeted bio-imaging, (2) prevention of premature drug release and (3) bio-responsive drug release. Bioresponsive gate keeping ability of CQDs has been reported for the first time. Inexpensive and ambient synthesis of CQDs from sugarcane waste and their fitness for exploitation in bioresponsive theranostics have been demonstrated successfully for the first time. DOX loaded nano-carrier releases the drug on exposure to the mimicked intracellular cancerous environment i.e., acidic pH and elevated levels of glutathione (GSH). The fluorescence and release kinetics studies show that the green fluorescent CQDs improve bio-imaging effectively preventing the premature release of drug and bioresponsive.

Acknowledgement

The authors are grateful to Anurag Shukla and Avtar Singh for cell imaging on HeLa cells. Omkar Singh and Sailaja Krishnamurty are acknowledged for fruitful discussions. RP acknowledges the UGC, New Delhi for Senior Research Fellowship. This work is supported by the grants under projects OLP002626 (CSIR-EMPOWER) and MLP 029226.

Notes and references

1 J. Wang, C. F. Wang and S. Chen, *Angew. Chem. Int. Ed*., 2012, **51**, 9297.
2 S. Y. Lim, W. Shen and Z. Gao, *Chem. Soc. Rev.,* 2015, **44**, 362.
3 S. Alberti, G. J. A. A. Soler-Illia and O. Azzaroni, *Chem. Commun*., 2015, **51**, 6050.
4 C. A. Lorenzo and A. Concheiro, *Chem. Commun*., 2014, **50**, 7743.
5 Y. Zhang, Y. Zhao, A. Yermukhambetova, Z. Bakenov and P. Chen, *J. Mater. Chem. A,* 2013, **1**, 295.
6 D. Peer, J. M. Karp, S. Hong, O. C. Farokhzad, R. Margalit and Robert Langer, *nat. nanotechnol*, 2007, **2**, 751.
7 L. Tang and J. Cheng, *Nano Today*, 2013, **8**, 290.

8 W. X. Mai and H. Meng, *Integr. Biol.,* 2013, **5**, 19.
9 I. Slowing, B.G. Trewyn, V.S. Lin, *J. Am. Chem. Soc.,* 2006, **128**, 14792.
10 Y. L. Zhao, Z. Li, S. Kabehie, Y. Y. Botros, J. F. Stoddart, and J. I. Zink, *J. Am. Chem. Soc.,* 2006, **132**, 13016.
11 Z. Li, J. C. Barnes, A. Bosoy, J. F. Stoddart and J. I. Zink, *Chem. Soc. Rev.*, 2012, **41**, 2590.
12 M. R. Melloa, D. Phanonb, G. Q. Silveira, P. L. Llewellyn, C. M. Ronconi, *Micropor. Mesopor. Mat.*, 2011, **143**, 174.
13 O. S. Kushwaha, C. V. Avadhani and R. P. Singh, *Carbohyd Polym,* 2015, **123**, 164.
14 J. L. Vivero-Escoto, I. I. Slowing, B. G. Trewyn and V. S.-Y. Lin, *Small*, 2010, **6**, 1952.
15 K. K. Coti, M. E. Belowich, M. Liong, M. W. Ambrogio, Y. A. Lau, H. A. Khatib, J. I. Zink, N. M. Khashab and J. F. Stoddart, *Nanoscale,* 2009, **1**, 16.
16 M. Vallet-Regı, F. Balas and D. Arcos, *Angew. Chem. Int. Ed.,* 2007, **46**, 7548.
17 M. Manzano and M. Vallet-Regi, *J. Mater. Chem.,* 2010, **20**, 5593.
18 N. Singh, A. Karambelkar, L. Gu, K. Lin, J. S. Miller, C. S. Chen, M. J. Sailor and S. N. Bhatia, *J. Am. Chem. Soc.,* 2011, **133**, 19582.
19 J. E. Lee, N. Lee, T. Kim, J. Kim and T. Hyeon, *Acc. Chem. Res.*, 2011, **44**, 893.
20 Y. Piao, A. Burns, J. Kim, U. Wiesner and T. Hyeon, *Adv. Funct. Mater.*, 2008, **18**, 3745.
21 J. M. Rosenholm, V. Mamaeva, C. Sahlgren, M. Lindén, *Nanomedicine*, 2012, **7**, 111.
22 S. Niedermayer, V. Weiss, A. Herrmann, A. Schmidt, S. Datz, K. Muller, E. Wagner, T. Bein and C. Brauchle, *Nanoscale*, 2015, **7**, 7953.
23 H. Meng, M. Xue, T. Xia, Y. Zhao, F. Tamanoi, J. F. Stoddart, J. I. Zink and A. E. Nel, *J. Am. Chem. Soc.*, 2010, **132**, 12690.
24 C. Argyo, V. Weiss, C. Bräuchle and T. Bein, *Chem. Mater.,* 2014, **26**, 435.
25 S. Mackowiak, A. Schmidt, V. Weiss, C. Argyo, C. V. Schirnding, T. Bein, C. Bräuchle, *Nano Lett.,* 2013, **13**, 2576.
26 I. R. Fernando, D. P. Ferris, M. Frasconi, D. Malin, E. Strekalova, M. D. Yilmaz, M. W. Ambrogio, M. M. Algaradah, M. P. Hong, X. Chen, M. S. Nassar, Y. Y. Botros, V. L. Cryns and J. F. Stoddart, *Nanoscale*, 2015,**7**, 7178.
27 N. K. Mal, M. Fujiwara, Y. Tanaka, T. Taguchi and M. Matsukata, *Chem. Mater.,* 2003, **15**, 3385.
28 M. W. Ambrogio, T. A. Pecorelli, K. Patel, N. M. Khashab, A. Trabolsi, H. A. Khatib, Y. Y. Botros, J. I. Zink and J. F. Stoddarrt, *Org. Lett.,* 2010, **12**, 3304.
29 N. Song and Y. W. Yang, *Chem. Soc. Rev*., 2015, **44**, 3474.
30 S. Giri, B. G. Trewyn, M. P. Stellmaker and V. S. Lin, *Angew. Chem. Int. Ed*., 2005, **117**, 5166.
31 H. Li, L. L. Tan, P. Jia, Q. L. Li, Y. L. Sun, J. Zhang, Y. Q. Ning, J. Yu and Y. W. Yang, *Chem. Sci.,* 2014, **5**, 2804.
32 T. Chen, H. Yu, N. Yang, M. Wang, C. Dinga and J. Fu, *J. Mater. Chem. B,* 2014, **2**, 4979.
33 L. Zhou, Z. H. Li, Z. Liu, J. S. Ren and X. G. Qu, *Langmuir,* 2013, **29**, 6396.
34 Z. Li, J. C. Barnes, A. Bosoy, J. F. Stoddart and J. I. Zink, *Chem. Soc. Rev.,* 2012, **41**, 2590.
35 A. Mewada, S. Pandey, S. Shinde, N. Mishra, G. Oza, M. Thakur and M. Sharon, *Mater. Sci. Eng. C*, 2013, **33**, 2914.
36 S. N. Baker and G. A. Baker, *Angew. Chem. Int. Ed.,* 2010, **49**, 6726.
37 J. H. Shen, Y. H. Zhu, X. L. Yang and C. Z. Li, *Chem. Commun.,* 2012, **48**, 3686.
38 S. Y. Lim, W. Shen and Z. Gao, Chem. Soc. Rev., 2015, **44**, 362.
39 J. Shen, Y. Zhu, X. Yang and C. Li, *Chem. Commun.,* 2012, **48**, 3686.
40 U. R. Genger, M. Grabolle, S. C. Jaricot, R. Nitschke and T. Nann, *Nat. Methods*, 2008, **5**, 763.
41 J. Liu, L. Cao, G. E. LeCroy, P. Wang, M. J. Meziani, Y. Dong, Y. Liu, P. G. Luo and Y. P. Sun, *ACS Appl. Mater. Interfaces*, 2015, **7**, 19439.
42 Y. Dong, N. Zhou, X. Lin, J. Lin, Y. Chi and G. Chen, *Chem. Mater.,* 2010, **22**, 5895.
43 X. Y. Xu, R. Ray, Y. L. Gu, H. J. Ploehn, L. Gearheart, K. Raker and W. A. Scrivens, *J. Am. Chem. Soc.*, 2004, **126**, 12736.
44 A. Mewada, S. Pandey, M. Thakur, M. Sharon, D. Jadhav and M. Sharon, *J. Mater. Chem. B*, 2014, **2**, 698.
45 S. J. Zhu, J. H. Zhang, C. Y. Qiao, S. J. Tang, Y. F. Li, W. J. Yuan, B. Li, L. Tian, F. Liu, R. Hu, H. N. Gao, H. T. Wei, H. Zhang, H. C. Sun and B. Yang, *Chem. Commun*., 2011, **47**, 6858.
46 J. Zhao, G. F. Chen, L. Zhua and G. X. Li, *Electrochem. Commun.,* 2011, **13**, 31.
47 L. Cao, X. Wang, M. J. Meziani, F. Lu, H. Wang, P. G. Luo, Y. Lin, B. A. Harruff, L. M. Veca, D. Murray, S. Y. Xie and Y. P. Sun, *J. Am. Chem. Soc*., 2007, **129**, 11318.
48 B. R. Selvi, D. Jagadeesan, B. S. Suma, G. Nagashankar, M. Arif, K. Balasubramanyam, M. Eswaramoorthy and T. K. Kundu, *Nano Lett.,* 2008, **8**, 3182.
49 Q. L. Zhao, Z. L. Zhang, B. H. Huang, J. Peng, M. Zhang and D. W. Pang, *Chem. Commun*., 2008, **5**, 116.
50 H. Liu, T. Ye and C. Mao, *Angew. Chem. Int. Ed.,* 2007, **46**, 6473.
51 Y. Li, Y. Hu, Y. Zhao, G. Q. Shi, L. E. Deng, Y. B. Hou and L. T. Qu, *Adv. Mater.,* 2011, **23**, 776.
52 J. H. Shen, Y. H. Zhu, C. Chen, X. L. Yang and C. Z. Li, *Chem. Commun.*, 2011, **47**, 2580.
53 R. Liu, D. Wu, X. Feng and K. Müllen, *J. Am. Chem. Soc.,* 2011, **133**, 15221.
54 J. Peng, W. Gao, B. K. Gupta, Z. Liu, R. R. Aburto, L. Ge, L. Song, L. B. Alemany, X. Zhan, G. Gao, S. A. Vithayathil, B. A. Kaipparettu, A. A. Marti, T. Hayashi, J. J. Zhu and P. M. Ajayan, *Nano Lett.,* 2012, **12**, 844.
55 S. Takae, K. Miyata, M. Oba, T. Ishii, N. Nishiyama, K. Itaka, Y. Yamasaki, H. Koyama and K. Kataoka, *J. Am. Chem. Soc.,* 2008, **130**, 6001.
56 H. Kim, S. Kim, C. Park, H. Lee, H. J. Park and C. Kim, *Adv. Mater.,* 2010, **22**, 4280.
57 Y.-L. Li, L. Zhu, Z. Liu, R. Cheng, F. Meng, J.-H. Cui, S. J. Ji and Z. Zhong, *Angew. Chem. Int. Ed.,* 2009, **48**, 9914.
58 G. Saito, J. A. Swanson, K. D. Lee, *Adv. Drug Deliv. Rev.,* 2003, **55**, 199.
59 Q. Zhao, H. Geng, Y. Wang, Y. Gao, J. Huang, Y. Wang, J. Zhang and S. Wang, *ACS Appl. Mater. Interfaces*, 2014, **6**, 20290.
60 J. Zhou, N. Hao, T. D. Zoyza, M. Yan and O. Ramström, *Chem. Commun.,* 2015, **51**, 9833.
61 M. H. Lee, Z. Yang, C. W. Lim, Y. H. Lee, S. Dongbang, C. Kang and J. S. Kim, *Chem. Rev.,* 2013, **113**, 5071.
62 S. K. Jhajharia and K. Selvaraj, *Nanoscale*, 2015,**7**, 19705.
63 M. Chen, X. He, K. Wang, D. He, S. Yang, P. Qiu and S. Chen, *J. Mater. Chem. B,* 2014, **2**, 428.
64 Y. L. Zhao, Z. Li, S. Kabehie, Y. Y. Botros, J. F. Stoddart and J. I. Zink, *J. Am. Chem. Soc.,* 2010, **132**, 13016.
65 H. Meng, M. Xue, T. Xia,Y. L. Zhao, F. Tamanoi, J. F. Stoddart, J. I. Zink and A. E. Nel, *J. Am. Chem. Soc.,* 2010, **132**, 12.